Solar Energy 214 (2021) 478–490

Contents lists available at ScienceDirect

Solar Energy

journal homepage: www.elsevier.com/locate/solener

Experimental investigation of transpired solar collectors with/without phase change materials

A.S. Bejan, C. Teodosiu *, C.V. Croitoru, T. Catalina, I. Nastase

Faculty of Building Services and Equipment, CAMBI Research Center, Technical University of Civil Engineering, Bucharest 020396, Romania

ARTICLE INFO

Keywords:
Transpired Solar Collectors
Phase Change Materials
Experimental measurements

ABSTRACT

Transpired opaque Solar Collectors (TSCs) have been often used in buildings (e.g. for direct heating of the outside air) due to their efficiency. In addition, one way to improve their efficiency is to integrate Phase Change Materials (PCMs). As a result, the goal of this study is to thoroughly investigate the behavior of TSCs with integrated PCMs in comparison with TSCs without PCMs. Therefore, based on an experimental approach carried out in the laboratory, we determined the performances of two TSCs (with lobed perforations) of around 2 m^2 each, one of them containing approximately 15.1 kg of organic PCM (commercial paraffin RT35). The data achieved show the superiority of the TSC with PCM: the maximum overall efficiency is improved by almost 6%; the maximum heating capacity is approximately 7.7% higher and during the cooling/PCM discharge period, the average heating capacity is over 5 times higher; more than 17% supplementary energy during the 9 h of operation; the average coefficient of performance is 16.4% higher; the "useful time of operation" is over 86% longer (meaning almost 4 h more). Consequently, the prototype of TSC with PCM analyzed in this study has led to promising results. Nevertheless, future work is required to improve the configuration of the TSC with PCM in order to enhance the interaction between the air within the TSC and the PCM. Moreover, the TSC with the PCM should be tested under real operating conditions (integrated in buildings) for longer periods of time.

1. Introduction

Despite the fact that, according to a renewed IEA (International Energy Agency) report (IEA, 2020), the global energy demand is expected to decline by 6% in 2020 and, consequently, global CO_2 emissions are anticipated to contract by 8% this year, it is believed that the upward trend of energy consumption will resume its natural course as it was anticipated by previous studies, e.g. growth of world energy demand by 20% to 2040 (Exxon, 2019), or even by 50% to 2050 (US EIA, 2019).

On the other hand, all global energy scenarios' outputs and outlooks are taking into account the fact that renewable energy sources would have an increasingly important share in covering this higher world energy demand. The share of renewable energy in the total primary energy consumption of the world is supposed to rise to over 40% by 2040, from 25% in 2018 IEA, 2018). Fortunately, these assumptions lead to the conclusion that renewable energy will play a major role in decreasing greenhouse gas emissions on short and long term (Gielen et al., 2019). Furthermore, even in this unfortunate pandemic context, the only energy source estimated to increase in 2020 is renewables (IEA, 2020).

In this context, it should be noted that buildings are among the main energy consumption sectors since buildings account for 36% of global final energy use and 39% of total greenhouse gas emissions (UN Environment and IEA, 2017). It is one of the reasons why the building sector enjoys a special interest regarding the implementation of energy efficiency solutions and the use of renewable energy sources.

It is also worth noting that among the renewable energy sources used in buildings, solar energy plays an extremely important role. For instance, recent data show that the total capacity of solar thermal installations at the end of 2019 was 479 GWth (Weiss et al., 2020). This is the equivalent of almost 42 million tons of oil savings and more than 135 million tons of CO_2 emissions reduction (Weiss et al., 2020).

Although solar water collectors are the most widely used today, air collectors have a number of advantages: there is no risk of frost and they have a lower impact on the environment (Reichl et al., 2015). Furthermore, according to Goyal et al. (1998) solar thermal air collectors can supply an air temperature of up to 65° C. In this context, it is worth mentioning that the total solar air collectors' area in operation in the

* Corresponding author.
E-mail address: catalin.teodosiu@utcb.ro (C. Teodosiu).

https://doi.org/10.1016/j.solener.2020.11.035
Received 3 September 2020; Received in revised form 16 October 2020; Accepted 11 November 2020
Available online 25 December 2020

world, by the end of 2017, exceeded 1.5 million square meters (Weiss et al., 2020).

On the other hand, depending on the construction characteristics, solar air collectors can be classified in several ways. Briefly, solar air collectors can be grouped into two main categories (Hami et al., 2012; Lai and Hokoi, 2015): solar collectors in which the absorber element is flat and solar collectors in which the absorber element is perforated ("transpired"). It should be also mentioned that both types can be with or without glazing. In addition, both types of collectors may contain several coils to increase heat transfer and also both types of collectors may be with or without thermal energy storage media (inertial materials).

According to numerous specialized studies (Dymond and Kutscher, 1997; Leon and Kumar, 2007; Alkilani et al., 2011; Nkwetta and Haghighat, 2014; Paya-Marin et al., 2015; Zhang et al., 2016a, 2016b; Ciriminna et al., 2017), solar air collectors can be used for the following applications, having an important potential to reduce energy consumption and operating costs (Leon and Kumar, 2007): heating and cooling of buildings, maintaining a guard temperature in industrial spaces, food drying, preheating of fresh air, heating and drying of greenhouses, improving the efficiency of photovoltaic systems.

In this context, it is worth mentioning that perforated plate ("transpired") opaque solar collectors (briefly called as "TSCs") have been often used in buildings due to their efficiency and low implementation costs (Wang et al., 2017). For instance, TSCs have been successfully implemented in large North American and European buildings, having the potential to replace glazed solar collectors (Leon and Kumar, 2007). Furthermore, according to Gunnewiek et al. (2002), TSCs are particularly recommended for direct heating of the outside air, these type of solar collectors being able to achieve efficiencies of up to 72%. The presence of perforations in the absorber plate allows the recovery of heat lost by convection and radiation at the surface of the plate (Cordeau and Barrington, 2011; Chan et al., 2014). According to Chan et al. (2014), the efficiency of TSCs is even 50% higher than that of flat plate solar collectors under similar working conditions. Another study dealing with geometrical optimization of TSCs, Tajdaran et al. (2020), revealed that their performance could be improved by 43% even when 28% less material is used, this being an interesting finding especially for regions with reduced solar radiation. Peci et al. (2020), based on experimental studies concerning buildings refurbishment, came to the conclusion that for more than 74% of the 28 days taken into account in their study, the ventilation heating demand would be covered in winter for continental cold and dry climate of Cordoba (Spain) by using modules of unglazed transpired collector façade. Investigations carried out by Li et al. (2020) showed that the solution based on the integration of TSCs in the ventilation system of school classrooms in winter led to the best performances in terms of energy savings, environmental protection and economic impact in comparison with other solutions (e.g. the air is heated with air conditioners or electric heaters).

Concerning the economic aspects, according to Paya-Marin (2017), TSCs are a cost-effective solution. Paya-Marin (2017) conducted an economic study on the implementation of opaque solar collectors and the analysis of TSCs, taking into account the installation and operation costs, revealed that the depreciation period is approximately four years. The TSCs may have also lower lifetime costs according to Reichl et al. (2015).

In addition, TSCs can integrate other methods of increasing energy efficiency, e.g. photovoltaic panels or phase change materials ("PCMs") (Shuklaa et al., 2012).

Concerning the integration of PCMs within TSCs, according to Navarro et al. (2016) solar energy systems combined with inertial elements are a very good alternative to conventional systems, the integration of PCMs storing latent heat leading to a greater impact than conventional materials. In addition, Tyagi and Buddhi (2007) showed that the same performances are achieved with less quantity of PCMs when these materials are used in Trombe walls to replace masonry and classical materials. From this point of view, Bourdeau (1980) stated that 8.1 cm of PCMs (with phase change temperature at 29 °C) determines performances similar to 40 cm of masonry. Furthermore, Qiu et al. (2019) pointed out that the efficiency of solar air collectors increases with the use of PCMs, and although the temperature of the air discharged from the collector is lower during the day (while PCMs accumulate energy), this is higher during the night when the stored energy by PCMs is released. The same phenomenon is observed by Goyal et al. (1998), who also noted that as the thickness of the thermal mass layer increases, the efficiency of the collector decreases, since the material stores and releases thermal energy over a longer period of time. In fact, the integration of PCMs in TSCs results in a longer operation time because it includes a time period even after the incident solar radiation disappears (Badescu et al., 2019). The data presented in another study concerning the implementation of a "PCM-based thermal storage control system integrated unglazed transpired collector" for pig barns (Moon and Kim, 2019) also highlight the contribution of PCMs to improving the behavior of TSC systems in this case: 22% daily average of heat storage efficiency (with maximum values up to 85%), temperature difference of 22.6 °C due to direct impact of PCM, and important effects on modifying heating time (e.g. heating directly during daytime as a result of decrease in the peak temperature of the supply air). Finally, Poole et al. (2018) methodically investigated the performance of a TSC-PCM system and its application for heating ventilation air. Their experimental results showed that the TSC-PCM system had the potential to store 34% of the total thermal energy used during the night to heat the air, for a week (in April), in the climate of Raleigh – North Carolina (USA). In addition, the TSC-PCM based thermal energy storage system studied by Poole et al. (2018) was able to supply, on average, air 4 °C warmer than the outside temperature during the night.

Based on these results, the aim of this study is to thoroughly assess the behavior of TSCs with integrated PCMs in comparison with TSCs without PCMs, given that more data is needed on the performance of TSCs with PCMs and how this equipment can be better used and integrated into buildings (e.g. better storing of the excess thermal energy during the day, extension of the operation time during the night). It should also be noted that the data obtained through this study will be used within an extensive research program on innovative solutions integrated in low energy buildings.

We first present the experimental set-up specially developed for the study of TSCs with/without PCMs, followed by the detailed analyses and discussion of the results.

2. Experimental set-up and methodology

The first stage of our experimental studies was represented by the construction of aluminum containers filled with PCMs (Bejan et al., 2018a). These canisters were first tested in small solar air collectors already used and validated in our laboratory (Bejan et al., 2017a, 2017b).

Then, these containers were integrated in large solar collectors presented below (see also Fig. 1). The TSC taken into consideration is composed of an absorber (aluminum plate, electrostatic painted in black, with an absorptivity of 0.96, and an emissivity of 0.88) with lobed perforations through which the outside air is sucked into a rectangular cavity with walls made of several layers: structural wood panel – Oriented Strand Board (OSB) inside, thermal insulation (4 cm) and OSB outside. The air gap created inside the solar collector has the following dimensions: 2000 × 1020 × 280 mm. The air is collected at the top of the system in a plenum (through an opening with dimensions of 830 × 150 mm) and then drawn through a circular air duct (180 mm) using a variable speed fan.

Fig. 2 shows the image of the solar collectors studied in our laboratory.

The geometry of the lobed holes is shown in Fig. 3. The pitch between the orifices is 20 mm, on each plate being approximately 5000

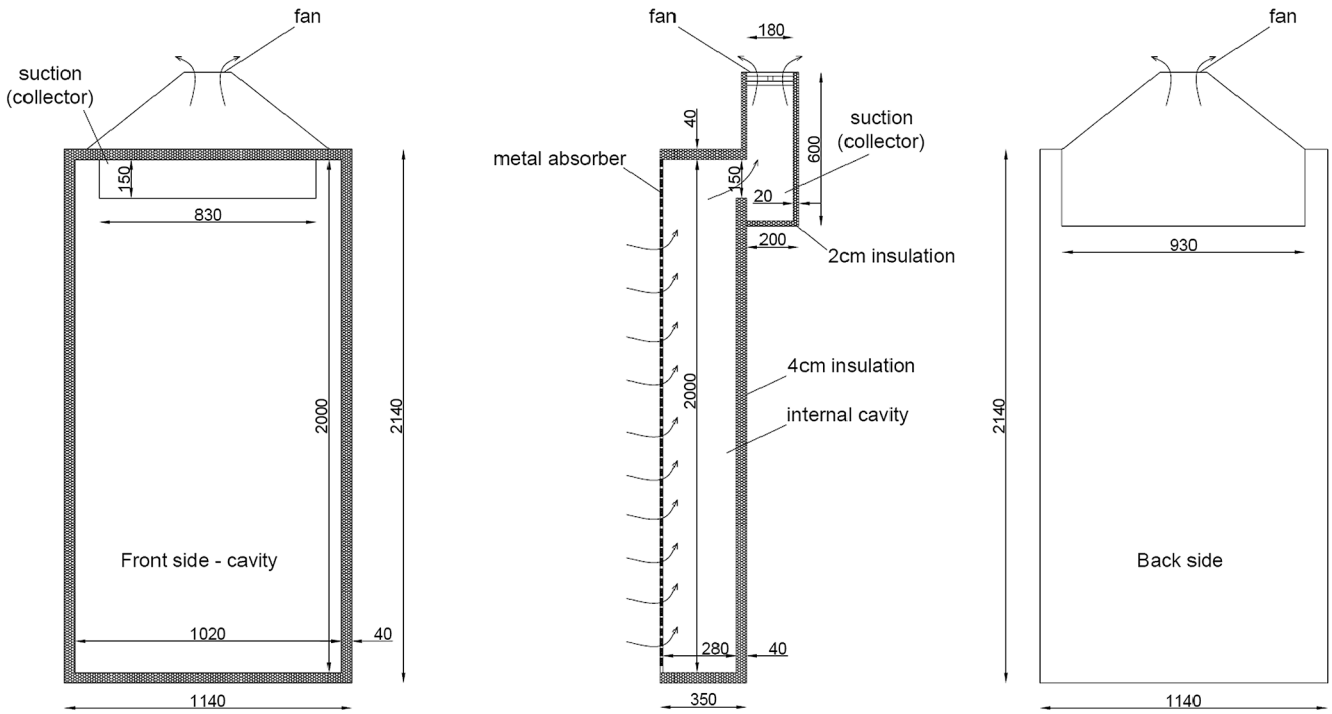

Fig. 1. TSC geometry, a – front view; b – section; c – rear view.

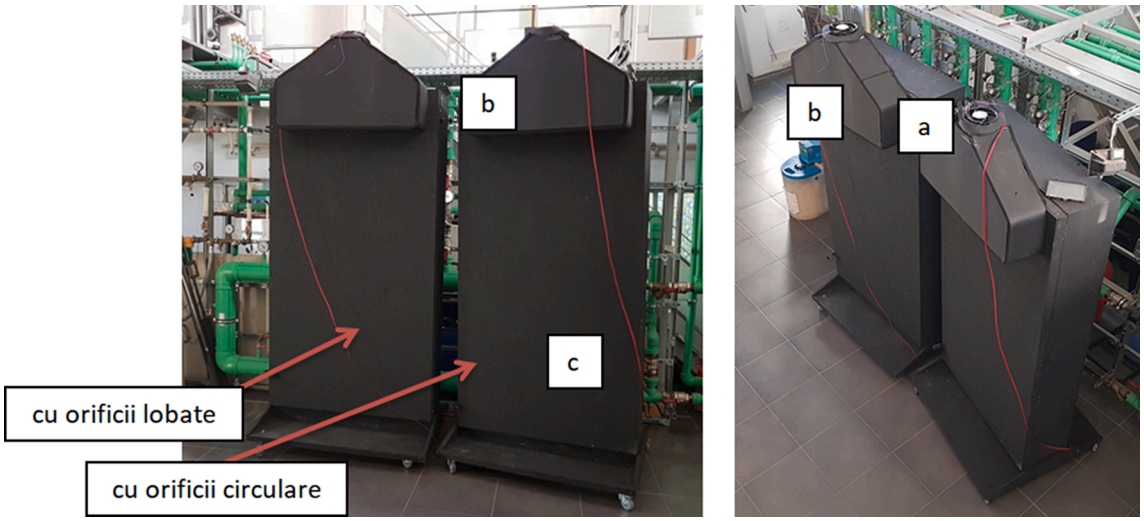

Fig. 2. TSCs picture (TSC 1 – without PCM; TSC 2 – with PCM), a – variable speed fan; b – air collector (plenum); c – rear wall.

Fig. 3. Absorber (metal plate) with lobed holes.

lobed holes (100 × 50), these being alternately placed: '+', 'x', '+', 'x'…

It should be noted that both types of holes have the same surface (19.635 mm^2) and the same equivalent diameter of 5 mm.

Fig. 4 details the TSC with lobed holes. It can be noticed, in the middle of the TSC cavity, the mobile assembly helping as support for PCMs (two detachable frames). 28 pieces of rectangular aluminum containers filled with PCMs are mounted on these two movable metal frames (Figs. 5 and 6).

It must be mentioned that there is a space for air flow of about 5 mm between the rectangular aluminum containers containing the PCMs. On the other hand, the containers material (aluminum) was used to increase the thermal conductivity, while their rectangular shape meets the requirements of the experimental stand configuration.

The PCM used is organic (commercial paraffin RT35) with the phase

Fig. 4. TSC with PCMs (construction details), a – absorber plate; b – air opening in the top part of the TSC cavity; c – air plenum; d – TSC rear wall; e – metal frame for PCMs.

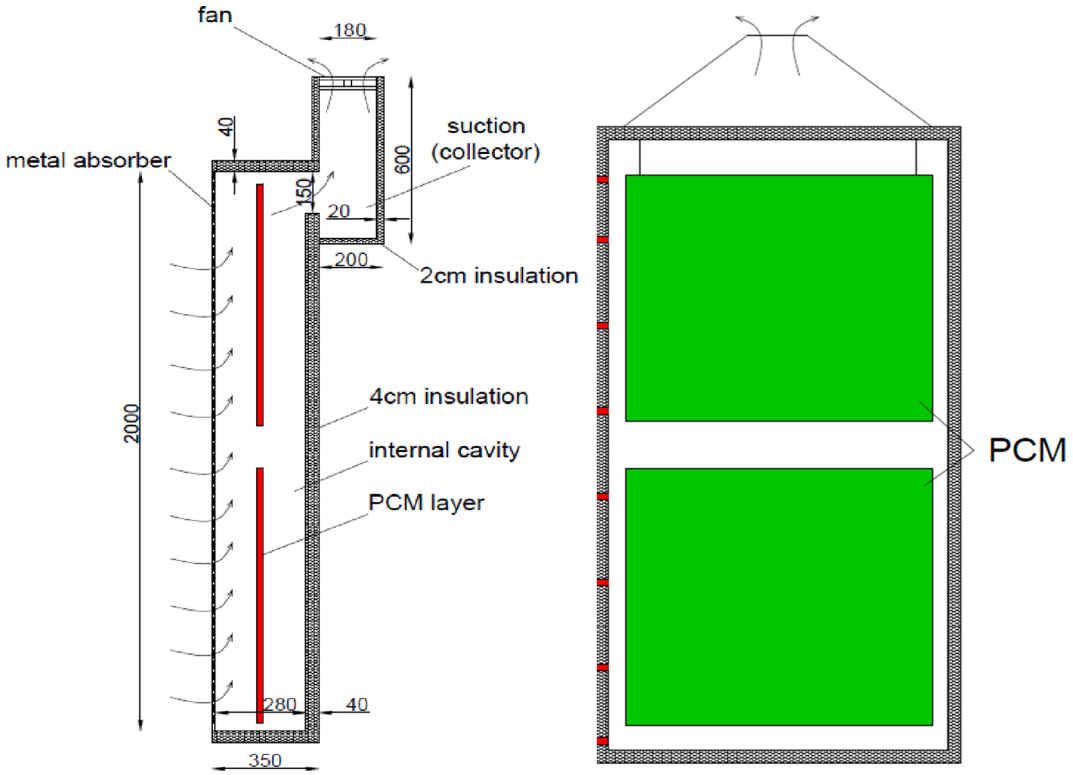

Fig. 5. Position of PCMs in the solar collector.

change temperature at 35 °C. Its choice is justified by the fact that this level of temperature complies with the average working temperature within the TSC cavity. The total amount of PCMs integrated in the 28 rectangular aluminum containers employed in the TSC is roughly 19.6 l when the paraffin RT35 is in liquid phase (around 15.1 kg). The properties of the PCM used (paraffin RT35) are shown in Table 1.

The experimental investigation was mainly based on 9 type K thermocouples (accuracy: ±0.2° C) distributed as follows (Fig. 7): 1 sensor for measuring the temperature on the absorber metal plate ($T_{metal\ plate}$); 1 sensor for measuring the temperature on the rear wall of the collector ($T_{back\ wall}$); 5 sensors that measure the thermal stratification in the air cavity within TSC (T30, T65, T100, T135, and T170); 1 sensor for measuring the outlet air temperature (T_{outlet}); 1 sensor for measuring the ambient temperature (T_{amb}).

It should be mentioned that the location of the 9 type K thermocouples is the same for both configurations: TSC with and without

Fig. 6. Picture of PCMs within the solar collector.

Table 1
PCM (paraffin RT35) properties (Rubitherm, 2019).

Characteristic	Value
melting area	29–36 °C
congealing area	36–31 °C
heat story capacity (26–41 °C) ± 7.5%	160 kJ/kg
specific heat capacity	2 kJ/kgK
density solid (la 15 °C)	0.86 kg/l
density liquid (la 45 °C)	0.77 kg/l
thermal conductivity (both phases)	0.2 W/mK
volume expansion	12.5%
Max. operation temperature	65 °C

embedded PCM.

In order to simulate the solar radiation, we used for the experimental set-up 8 halogen projectors (500 W each), located 0.8 m away from the TSC (Fig. 8). In this way, we obtained an intensity of the solar radiation of 800 W/m^2 (uniformly scattered on the absorber plate with lobed holes).

During the measurements the air flow through the solar collectors (with/without PCMs) was set to a value of 400 m^3/h, which corresponds to a specific air flow within the TSCs of 200 m^3/h/m^2. This high value of air flow rate has been taken into consideration as one of the expected applications of the solar collector systems from this study is for industrial buildings, characterized by large fresh air flow rates. In addition, the TSC configuration with lobed perforations taken into account within this study has been thoroughly optimized based on previous studies carried out in our laboratory. These studies showed that this geometry is 15% more efficient for air flow rates of around 220 m^3/h/m^2 (Croitoru et al., 2016a, 2016b).

Finally, the experimental data were continuously acquired throughout the experimental protocol and automatically recorded (time step of 60 s), based on data logger (Ahlborn Almemo 2890-9).

3. Experimental results

Following the experimental studies, extremely interesting aspects have been found.

The study was conducted for a total period of time of 570 min. For the first 250 min, the halogen lamps were switched on to simulate solar radiation and then they were switched off (for 320 min). Consequently, two stages of the experimental study can be clearly observed: the heating/loading stage of the PCMs (first 250 min) and the cooling/discharge stage of the PCMs (the next 320 min).

3.1. Analysis of temperature variations, thermal stratification and temperature rise within the TSCs with/without PCMs

Fig. 9 shows the temperature variations for five points in the case of the TSC without PCM: air outlet temperature (Toutlet), temperature in the middle of the collector (T 100 middle), temperature of the rear wall of the collector (T back wall), absorber plate temperature (T metal plate) and ambient air temperature (T ambient).

For instance, at an ambient temperature of 24 °C (minute 220), the exhaust air temperature is 33.4 °C, resulting in a temperature rise of 9.4 °C. At the same time, the temperature measured on the absorber plate is 48.9 °C, while the temperature on the rear wall of the TSC is 36.2 °C, and the temperature in the middle of the TSC is 32.1 °C.

As a result, it can be considered that the rear wall of the TSC acts as an inertial element, absorbing some of the energy, its temperature variation having higher values than the temperature in the TSC cavity or the air temperature at the outlet of the collector. After turning off the lamps, the values of the five analyzed temperatures are rapidly approaching, only the temperature of the TSC rear wall having a dephasing of about 120 min as shown in Fig. 9.

On the other hand, the temperature variations for the same five points taken into account are shown in Fig. 10 in the case of the TSC with PCM.

It can be noticed this time that at an ambient temperature of 24.2 °C (the same minute 220), the exhaust air temperature is 34.4 °C, resulting in air temperature increase of 10.2 °C within the TSC. At the same time, the temperature measured on the absorber plate is 50 °C, the temperature on the TSC rear wall is 33.9 °C, and the temperature in the middle of the solar collector is 35.9 °C.

In addition, it can be remarked that, unlike the previous case, the temperature of the TSC rear wall has lower values than the air

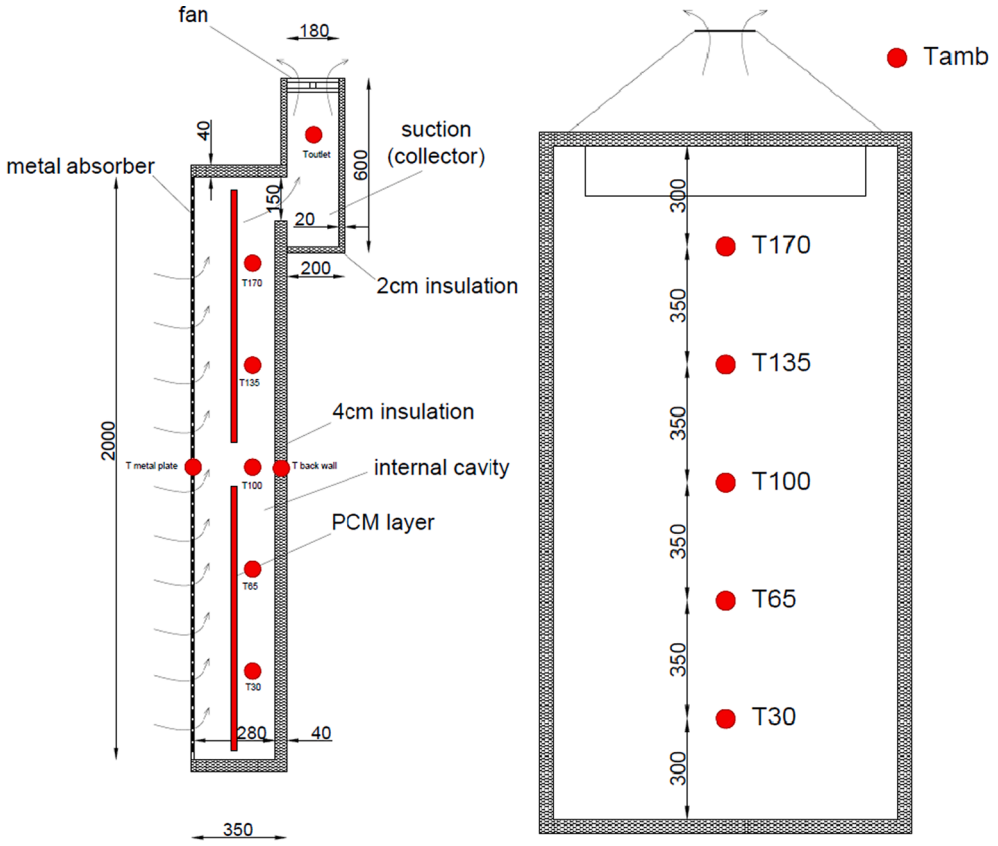

Fig. 7. Installation of the thermocouples within the experimental set-up.

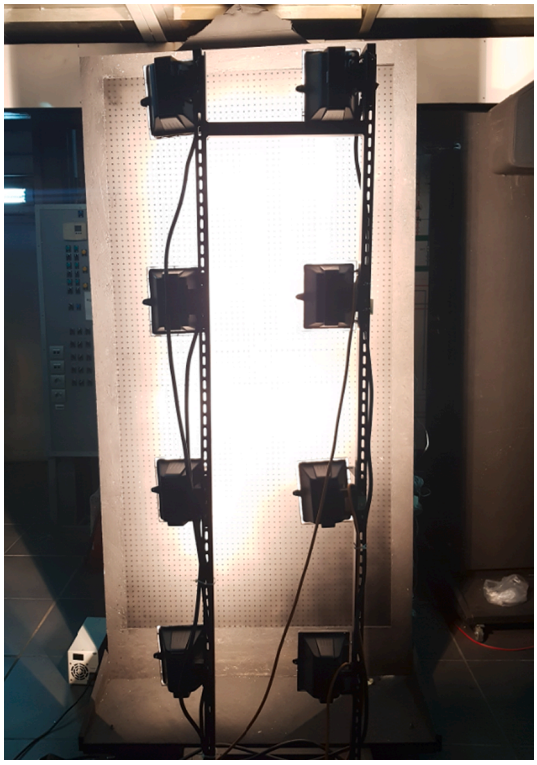

Fig. 8. Installation of the halogen projectors within the experimental set-up.

temperature in the middle of the cavity or at the exit of the solar collector, due to PCMs energy storage.

Another interesting finding is that the air temperature in the middle of the TSC cavity has lower values than in the previous situation because the air flow is modified within the TSC with PCM inside: the air circulation will principally occur in areas where there are no aluminum containers with PCM.

Moreover, the air outlet temperature is noticeably lower than the air temperature in the middle of the TSC with PCM, which indicates that the air flow takes place especially at the top of the solar collector in the case of this configuration. This hypothesis is also confirmed in other studies (Bejan et al., 2018b).

Furthermore, after turning off the halogen lamps, the temperature of the absorber plate quickly reaches the ambient air temperature, but it can be seen that the other temperatures have higher values due to the discharge of PCMs and they approach each other only towards the end of the measurements.

Fig. 11 shows a normal stratification of air temperatures in the TSC without PCM: the air temperature values increase towards its upper area (corresponding to the air exit from the solar collector). The biggest air temperature difference between the bottom and the top of the TSC is 2.1 °C, and, after turning off the lamps that simulate solar radiation, it can be observed a rapid equalization of all temperatures.

Instead, in the case of the TSC with PCM, the phenomenon is completely different (Fig. 12). Due to the air pressure losses in this configuration with PCM (Bejan et al., 2018b), the thermal stratification is much accentuated. On the other hand, it can be also appreciated that most of the air flow takes place in this case through the free spaces between the groups of PCM containers. In addition, the air temperature at the top at 170 cm (T170) is often lower than at 135 cm (T135).

It is also possible that the PCM does not completely melt in the lower part of the TSC. The biggest air temperature difference between the lower and the upper part of the TSC is double now with PCM (4.2 °C),

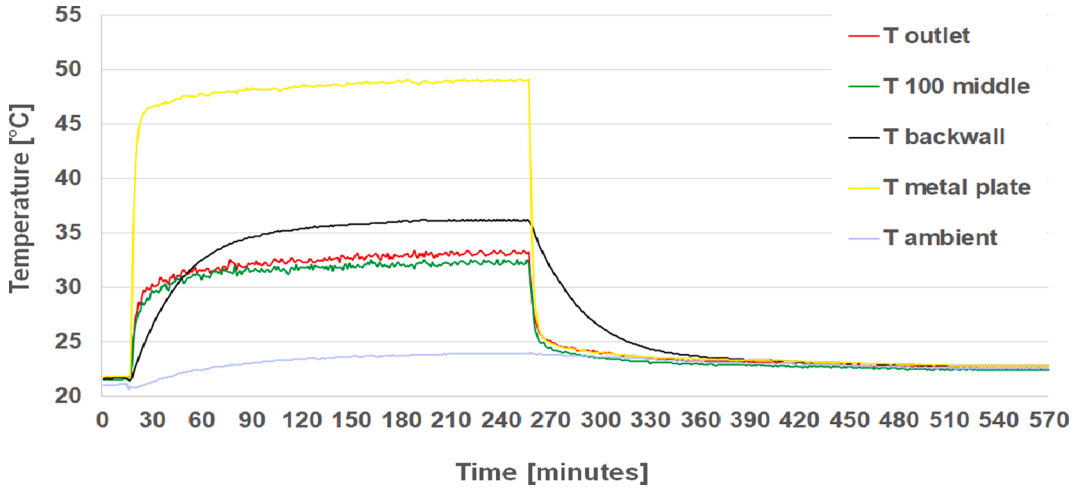

Fig. 9. TSC without PCM: temperature values in five reference points.

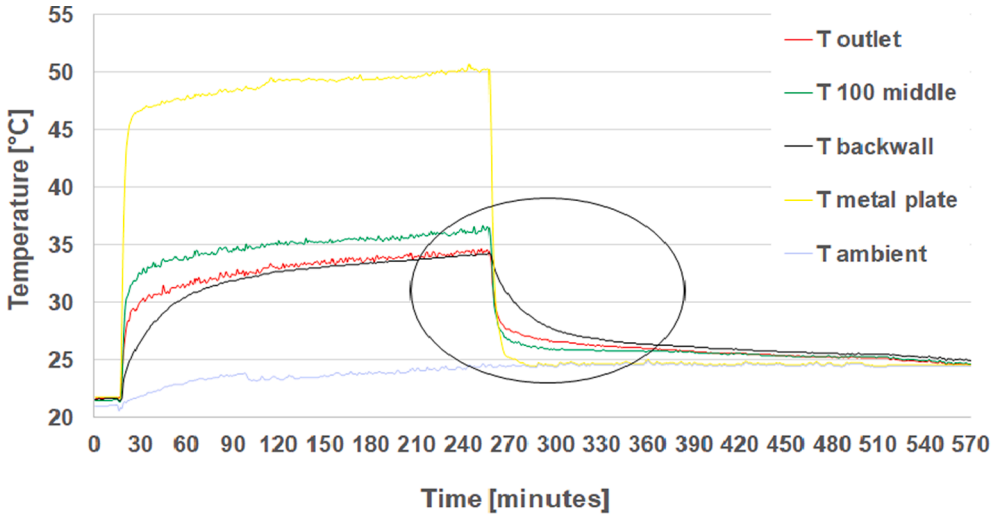

Fig. 10. TSC with PCM: temperature values in five reference points.

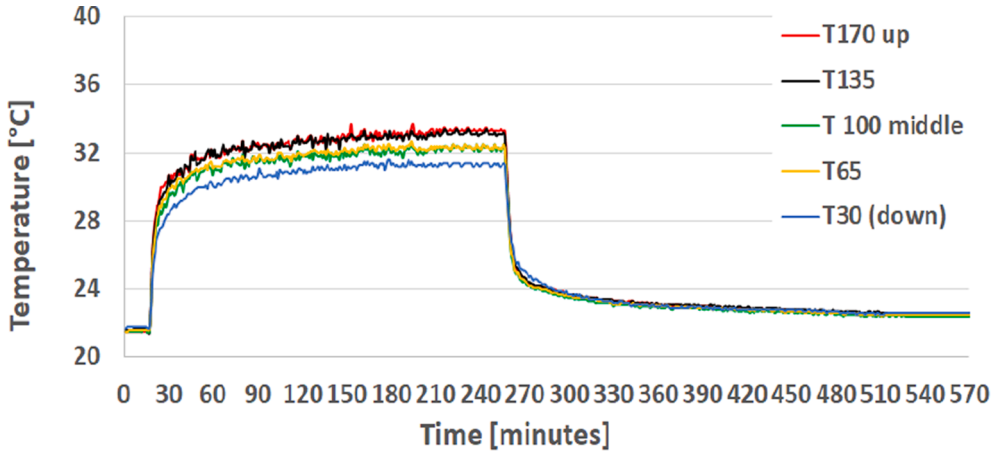

Fig. 11. Thermal stratification inside the TSC without PCM.

compared to the situation without PCM (2.1 °C).

Furthermore, this time, after switching off the halogen lamps, there is still a thermal stratification within the TSC (see Fig. 12) due to the slowly energy dissipation, accumulated by PCM.

The temperature difference between the TSC outlet air temperature and the ambient air temperature is classically calculated by the following formula:

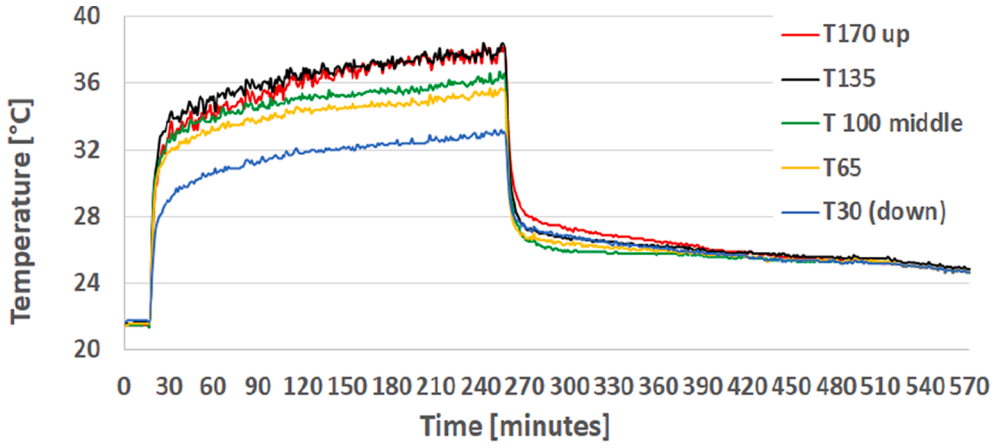

Fig. 12. Thermal stratification inside the TSC with PCM.

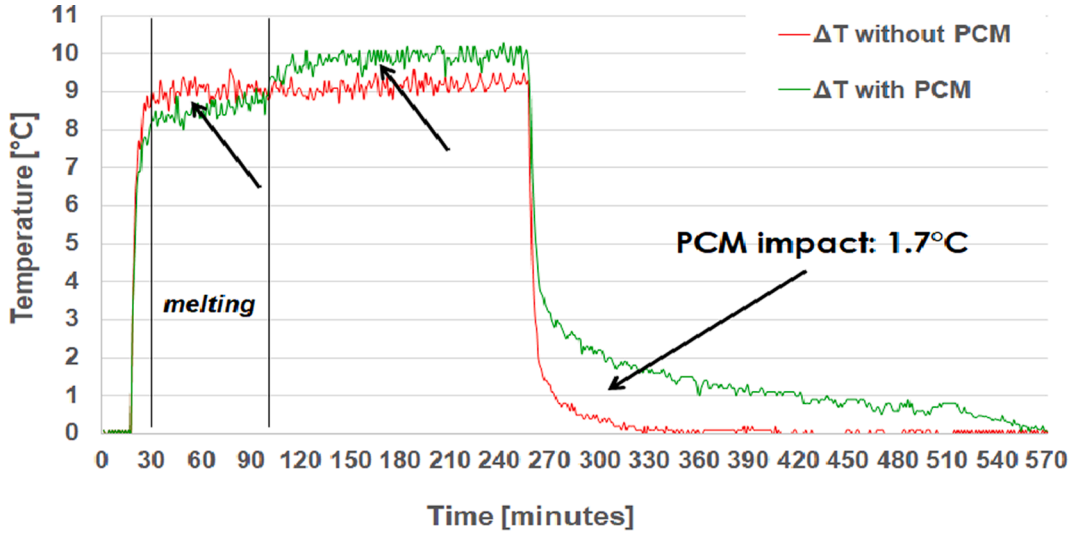

Fig. 13. Temperature difference: TSC outlet air temperature/TSC inlet (ambient) air temperature.

$$\Delta T = T_{outlet} - T_{ambient}\ [^{\circ}C] \quad (1)$$

Fig. 13 shows this temperature difference for both cases (TSC with and without integrated PCM). The impact of PCM is obvious: it can be clearly noticed the accumulation of energy during the heating period in which "solar radiation" is available and energy dissipation during the cooling period in which halogen lamps are switched off.

It can be seen that in the case of the TSC without PCM the temperature difference variation is relatively linear starting with minute 30 and reaches a maximum of 9.3 °C. On the other hand, in the case of the TSC with PCM, if at the beginning this variation has lower values than in the case without PCM (30–100 min) due to melting of PCM and energy accumulation, after 100 min the temperature difference is higher and reaches a maximum of 10.3 °C (10.7% more). Consequently, we can say that the melting phenomenon of the PCM is visible for 70 min.

It should also be noted that after the "solar radiation" is turned off, the outlet air temperature of the TSC without PCM quickly reaches the ambient air temperature (after about 50 min), while in the case of the TSC with PCM the outlet air temperature is higher for 300 min, until an equalization of the temperatures is noticeable. Moreover, after switching off the halogen lamps, the outlet air temperature from the TSC with PCM is higher than the ambient air temperature by up to 1.7 °C, reaching higher values even by 3 °C (especially at the beginning of the cooling process).

3.2. Analysis of thermal performances for the TSCs with/without PCMs

The rate of heat transfer $\dot{Q}$ [W] and the thermal energy Q [Wh] produced by solar collectors can be determined using the following formulas:

$$\dot{Q} = V\rho c_p \Delta T\ [W] \quad (2)$$

$$Q = \dot{Q}t\ [Wh] \quad (3)$$

where

V – air flow rate of the solar collector [m^3/s]; ρ – air density [kg/m^3]; c_p – air specific heat capacity [J/kg/°C]; ΔT – temperature difference between the outlet air temperature and the ambient air temperature [°C]; t – time [h].

Fig. 14 shows the variation of the heating capacity during the measurements for the two solar collectors taken into consideration: TSC with PCM and TSC without PCM.

Based on the values from Fig. 14, the maximum thermal power of the TSC without PCM is 1296.6 W (minute 188), while the TSC with PCM reaches a maximum of 1391.2 W (minute 242), meaning 7.7% more. On the other hand, as it can be seen, the maximum value is reached faster in the case of the TSC without PCM as it is expected due to the lack of

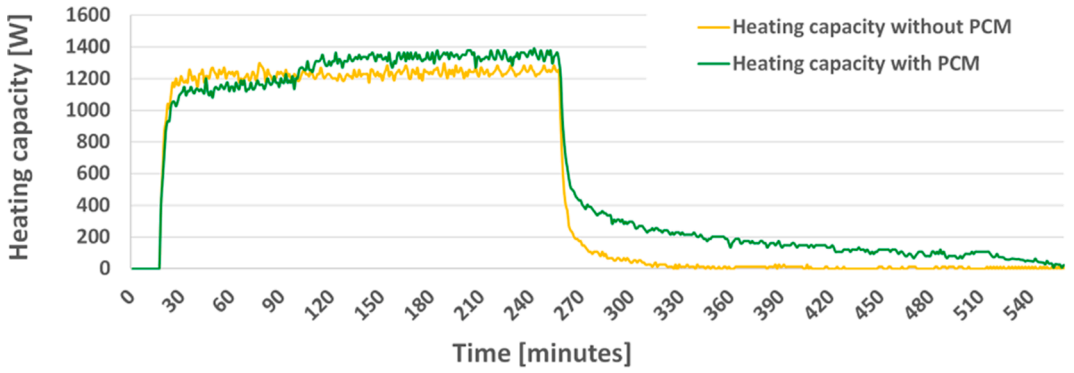

Fig. 14. TSC with/without PCM – heating capacity variation.

thermal inertia.

It is worthwhile to mention that during the heating/PCM charging period, the average heating capacity of the TSC with PCM is 1170 kW (590 W/m^2), approximately equal to that of the TSC without PCM which reaches a value of 1140 W (570 W/m^2), while during the cooling/PCM discharge period, the average value of the TSC with PCM is 169 W (84.6 W/m^2), almost 5.6 times higher than the TSC without PCM which has an average value of only 30 W (15.1 W/m^2). This important difference can be explained by the PCM dissipated energy in air within the TSC.

It can also be concluded that during the heating/PCM charging period the energy is accumulated faster (melting is evident between minute 30 and minute 100), while the solidification process occurs more slowly during the cooling/PCM discharge stage, though there is a period in which the process is more intense (between minute 257 and minute 573).

Fig. 15 shows the amount of thermal energy produced by the TSC with PCM and the TSC without PCM in each hour of operation during the measurements.

It can be seen that the TSC with PCM produces a maximum of 1345 Wh in one hour of operation (4th hour of operation), while the TSC without PCM delivers a maximum of 1245 Wh (at the same time, 4th hour of operation). The TSC with PCM supplies on average 655 Wh during the measurements, while the TSC without PCM generates on average 559 Wh.

During the heating/PCM charging period the quantity of energy produced by the TSC is similar in both cases, the differences appearing in the first part of the experimental studies when the PCMs change their state of aggregation. Basically, for all the heating stage, the TSC with PCM produces around 4650 Wh, approximately as much as the production of the TSC without PCM (about 4520 Wh). Instead, during the cooling/PCM discharging period of energy, the amount of energy produced by the TSC with PCM is sometimes even 11 times higher for certain hours. Globally, for the total operation time in cooling/PCM discharging, the TSC with PCM produces roughly 1260 Wh, meaning 2.5 times more than the TSC without PCM, which delivers only 510 Wh. Overall, for the entire period of the measurements, the total energy produced by the TSC without PCM is around 5030 Wh (2520 Wh/m^2), while the TSC with PCM generates roughly 5900 Wh (2950 Wh/m^2). This means 17.3% more energy for the TSC with PCM during the 9 h of operation. The explanation can be the fact that the aluminum containers filled with PCMs “catch” more energy from the solar radiation which enters through the lobe holes of the absorber metal plate, leading to improved heat transfer within the TSC in this case.

3.3. Analysis of the heat transfer effectiveness during the heating/PCM charging period

The heat exchange effectiveness of solar collectors can be assessed with the following expression (Wang et al., 2017):

$$\varepsilon = (T_{outlet} - T_{ambient})/(T_{metal\ plate} - T_{ambient}) \quad (4)$$

where: T_{outlet} – outlet air temperature [°C]; $T_{ambient}$ – ambient air temperature [°C]; $T_{metal\ plate}$ – absorber metal plate temperature [°C].

The variation in time of the heat transfer effectiveness for the two collectors (TSC without PCM and TSC with PCM) is shown in Fig. 16.

It can be remarked that the effectiveness of heat transfer in the case of the TSC with PCM has values constantly close to those of the TSC without PCM. The average effectiveness of the TSC with PCM is 36.8%,

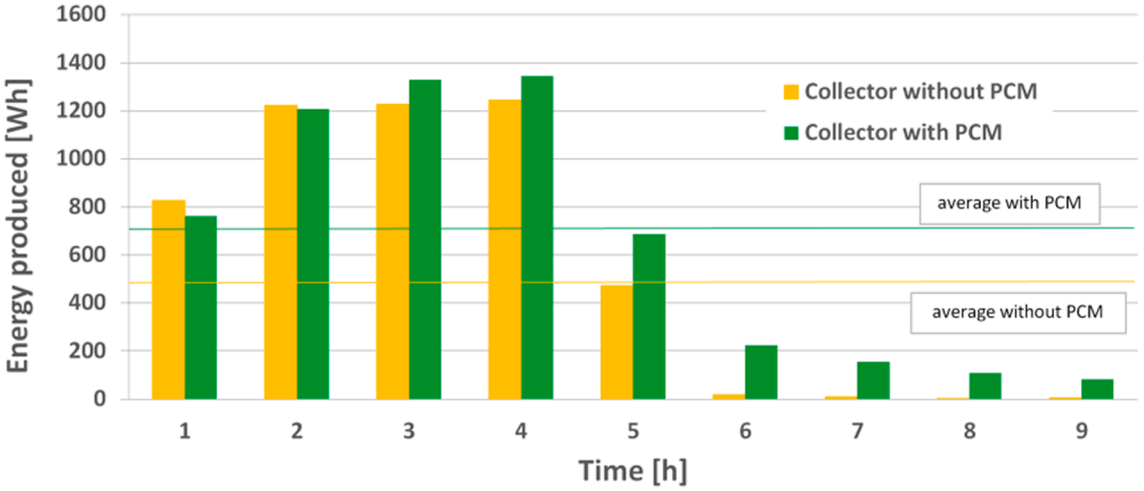

Fig. 15. TSC with/without PCM – thermal energy produced per hour.

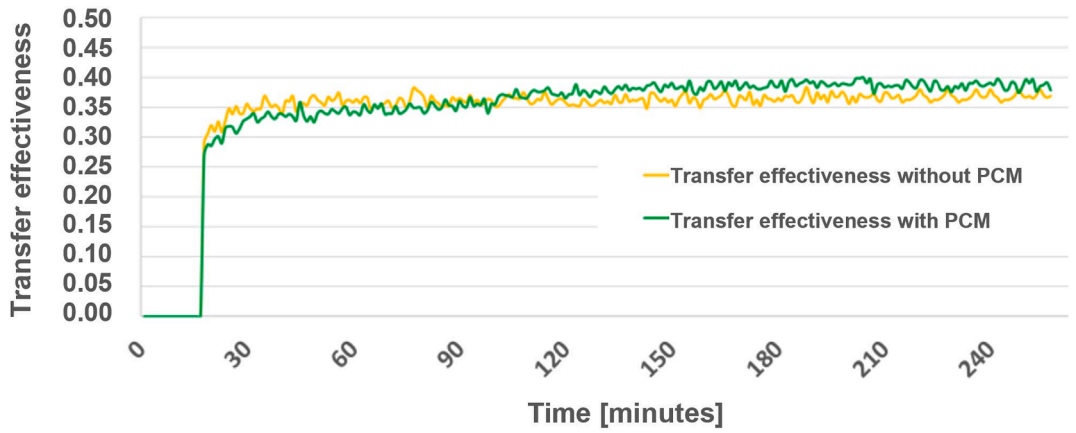

Fig. 16. Heat exchange effectiveness for TSC with/without PCM.

while the average effectiveness of the TSC without PCM is 36.13%. On the other hand, the melting process is once again visible, starting around the minute 18 and ending around the minute 100. After this minute, the trend of the heat exchange effectiveness is reversed: the TSC with PCM has now higher values (with a maximum value around 40%). The TSC without PCM reaches now a maximum value of 38.4%.

During the cooling//PCM discharge period, the effectiveness of the heat transfer cannot be evaluated as the temperature of the absorber plate becomes relatively equal to the ambient air temperature. On the other hand, the overall efficiency of the TSCs taken into account can be estimated by analyzing their coefficient of performance (COP), as it is presented below (see Section 3.5).

3.4. Analysis of the TSC global efficiency during the heating/PCM charging period

In order to assess the performance of solar collectors, another criteria is also used related to their global behavior (efficiency). This can be determined by the following formula (Wang et al., 2017):

$$\eta = \frac{\dot{Q}}{I_T A_S} \tag{5}$$

where: $\dot{Q}$ – rate of heat transfer for the solar collector [W], calculated according to Eq. (2); I_T – total incident solar radiation on the absorber of the solar collector [W/m^2]; A_S – absorber area of the solar collector [m^2].

Fig. 17 shows the variation of the efficiency for the TSC with/without PCM, based on Eq. (5). It can be seen that the efficiency of the TSC with PCM is lower in the first part of the heating/PCM charging process due to the accumulation of latent heat in the PCM, but after the PCM melting, its efficiency is higher due to improved heat transfer (PCM layer captures solar radiation through the lobe holes of the absorber metal plate and accumulates sensible heat when the PCM is already in the liquid state). As a result, the maximum and the average efficiency of the TSC with PCM are higher than those of the TSC without PCM (taken into consideration only the heating/PCM charging period): maximum efficiency – 86.9% versus 81% and average efficiency – 78.5% versus 76.2%.

3.5. Analysis of the coefficient of performance and the number of operating hours for TSC with/without PCM

As the heat transfer effectiveness and the overall efficiency of the solar collectors cannot be evaluated for the whole studied period including the cooling/PCM discharge stage (since in this case there is no solar radiation and the absorber plate temperature is almost equal to the ambient air temperature), it is necessary to take into account a new "indicator" for assessing the overall performance of the two solar collectors (with/without PCM).

For instance, Poole et al. (2018) proposed the use of a performance coefficient (COP) for solar collectors, defined, classically, as the ratio between the powers produced and demanded by the equipment (Eq. (6)).

$$COP = \frac{\dot{Q}}{\dot{Q}_{demand}} \tag{6}$$

where: $\dot{Q}$– produced power by the equipment, in this case heating capacity of the TSC according to Eq. (2) [W]; $\dot{Q}_{demand}$ – used power by the

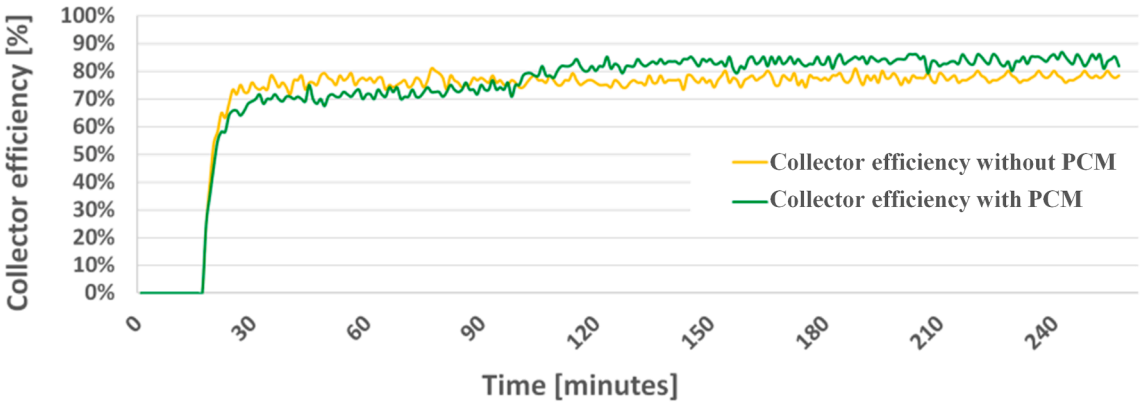

Fig. 17. Global efficiency for TSC with/without PCM.

equipment, in this case the fan electric power of the TSC [W].

Starting from Eq. (6), Fig. 18 shows the COP variation in time for the TSC with PCM and TSC without PCM, with the mention that the output power was determined according to Eq. (2) and the input power was 67 W (fan electric power).

It can be remarked that the evolution of these values is similar to that of the difference between the outlet air temperature and the ambient air temperature.

On the other hand, the maximum COP in the case of the TSC with PCM is 20.8, while the maximum COP of the TSC without PCM is 19.35. Moreover, during the heating/PCM charging period, the collector without PCM has an average COP close to that of the TSC with PCM: 17, compared to 17.52. Obviously, during the cooling/PCM discharge period, the TSC with PCM has a superior average COP: this time the COP is 5.6 times higher than the TSC without PCM (2.53 compared to 0.45).

It is also interesting to analyze the situation when the COP value of the solar collector falls below 1 as in this case the electric heating becomes more economically advantageous. Therefore, based on our results, from minute 289 the TSC without PCM should be turned off, while the TSC with PCM should be turned off from minute 524 (although this equipment can still provide heat).

Fig. 19 shows the average value of the COP in each hour of operation. It can be seen that the COP of the TSC with PCM is lower in the first part of the study, because the PCM accumulates energy, while after switching off the halogen lamps (no solar radiation anymore), the COP is considerably higher in favor of the TSC with PCM.

Totally, the average COP of the TSC without PCM is 7.9, while the average COP of the TSC with PCM is 9.2, respectively 10.6% higher.

As a conclusion, during the heating/PCM charging period, the energy is accumulated faster (melting is obvious between minute 18 and minute 100), while the solidification process occurs more slowly, during the whole cooling/PCM unloading stage. Therefore, the charging occurs quickly, being sustained by solar radiation, while the discharge of energy is slow and may require supplementary approaches to improve heat transfer.

Finally, the "useful time of operation" of the solar collector can be defined as the time interval in which the COP of the collector is supraunitary, in this case the equipment being more efficient than conventional electric heating. Fig. 20 shows this useful period of operation for the two solar collectors. In the case of the TSC without PCM, the COP has a value greater than 1 from minute 17 to minute 289, meaning 272 min of operation. Unlike the classic collector, the TSC with PCM has a supraunitary value of COP from minute 17 to minute 524, resulting in 507 min of operation. In conclusion, the TSC with PCM has a useful period of operation 86.4% longer than the TSC without PCM (it works 235 min longer, in the same time interval studied).

4. Conclusions

The prototype of TSC with PCM analyzed in this work has led to promising results in comparison with the same configuration of TSC without PCM:

- almost an extra degree was gained in terms of maximum temperature difference between the TSC outlet air temperature and the ambient air temperature (10.2 °C versus 9.4 °C);
- for about 5 h, the TSC outlet air temperature is higher (by up to 1.7 °C) during the cooling/PCM discharge period;
- the maximum heating capacity is approximately 7.7% higher (roughly 1390 W compared to 1300 W);
- during the cooling/PCM discharge period, the average heating capacity is over 5 times higher;
- more than 17% supplementary energy during the 9 h of operation (5900 Wh or 2950 Wh/m^2 compared to 5030 Wh or 2520 Wh/m^2);
- the maximum efficiency is improved by almost 6% (86.9% versus 81%);
- the average COP is 16.4% higher (9.2 versus 7.9);
- the "useful time of operation" is over 86% longer (meaning almost 4 h more).

From an economic point of view, the additional investments costs for TSC with PCM (compared to TSC without PCM) are recovered due to energy savings mentioned above over a period of approximately 5–6 years. This estimation is valid for the climate in Romania (approximately 180 days for the heating season) and taking into account the price of electricity of 0.12 euro/kWh. Furthermore, the contribution of TSC with PCM to the reduction of CO_2 emissions (compared to the equivalent solution without PCM) can also be estimated: around 47 kg/heating season. It is worth mentioning that the payback period predicted above may be shorter in the coming years as prices for commercial PCM are in a continuous decline due to their growing demand (Entrop et al., 2016). However, the economic analysis regarding the implementation of the TSC with PCM taken into account in this study must be deepened based on the data obtained for real operating conditions over long periods of time.

On the other hand, it was found that in the case of the TSC with PCM the air flow occurs mainly through the upper part of the solar collector leading to an unfavorable thermal stratification within the TSC. As a result, there is a possibility that the PCM at the bottom of the solar collector would not completely have melt.

Consequently, some future work is needed to improve the configuration of the TSC with PCM (e.g. by assembling a "chicane" in the middle of the air cavity to force the airflow toward the bottom of the solar collector leading to a better interaction between the air and the PCM from that zone).

Finally, it is also necessary to conduct the study over a longer period

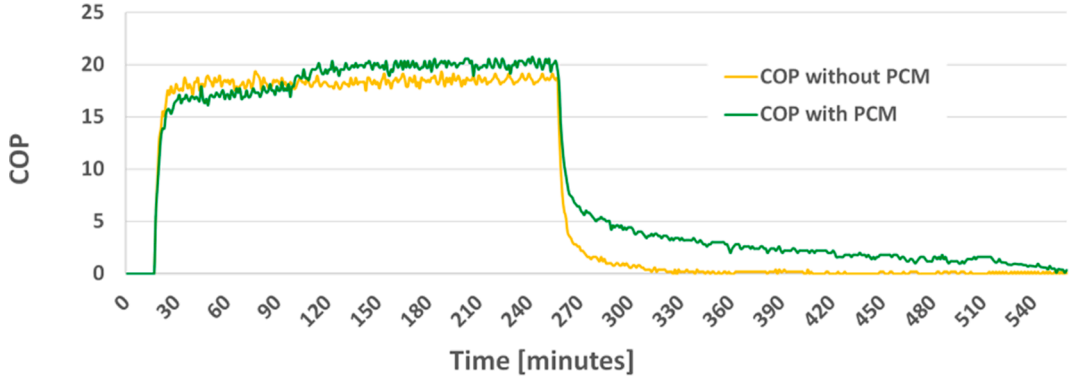

Fig. 18. COP for TSC with/without PCM.

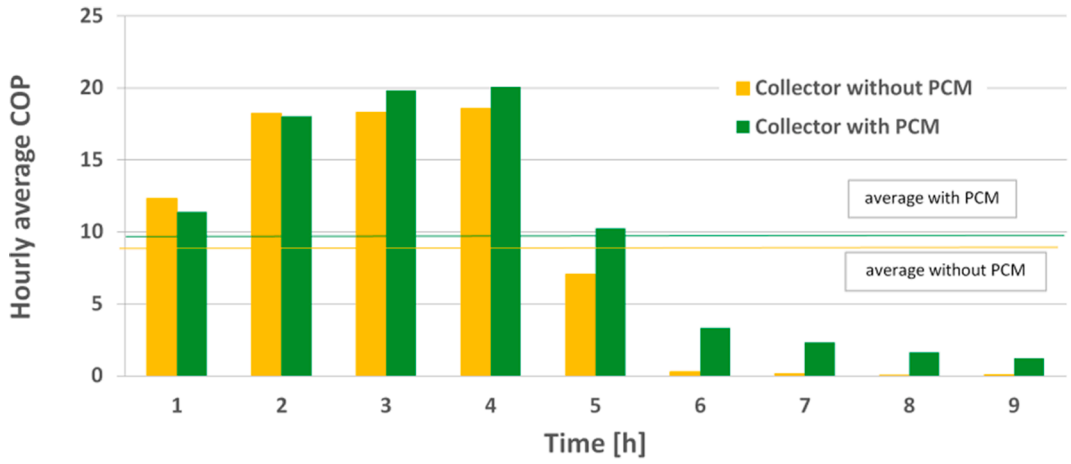

Fig. 19. Average hourly COP for TSC with/without PCM.

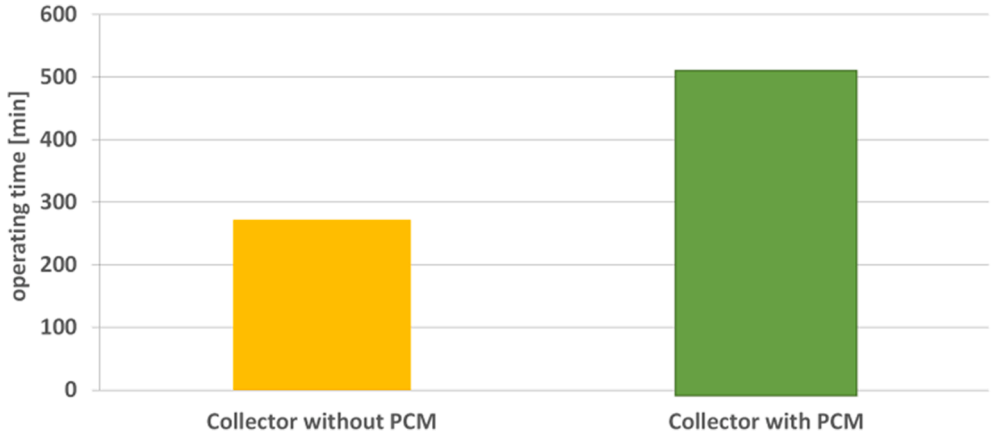

Fig. 20. Useful time of operation for TSC with/without PCM.

of time in order to thoroughly investigate the discharge of energy – phenomenon that requires a longer duration. In addition, it is compulsory to perform parametric studies in order to optimize the configuration of the TSC with PCM, as well as to analyze it for longer periods of time, in real operating conditions.

Declaration of Competing Interest

The authors declare that they have no known competing financial interests or personal relationships that could have appeared to influence the work reported in this paper.

Acknowledgement

This study was financed by Romanian National Authority for Scientific Research, project CIA-CLIM "Smart buildings adaptable to the climate change effects" PN-III-P1-1.2-PCCDI-2017-0391.

References

Alkilani, M.M., Sopian, K., Alghoul, M.A., Sohif, M., Ruslan, M.H., 2011. Review of solar air collectors with thermal storage units. Renew. Sustain. Energy Rev. 15 (3), 1476–1490. https://doi.org/10.1016/j.rser.2010.10.019.

Badescu, V., Ciocanea, A., Budea, S., Soriga, I., 2019. Regularizing the operation of unglazed transpired collectors by incorporating phase change materials. Energy Convers. Manage. 184, 681–708. https://doi.org/10.1016/j.enconman.2019.01.049.

Bejan, A.S., Labihi, A., Croitoru, C.V., Bode, F., Sandu, M., 2017. Experimental investigation of the performance of a transpired solar collector acting as a solar wall. In: Proceedings of the ISES Solar World Congress 2017, 29 October – 02 November 2017, Abu Dhabi, UAE. https://doi:10.18086/swc.2017.31.01.

Bejan, A.S., Croitoru, C.V., Bordianu, D., Labihi, A., Chehouani, H., 2017. Transpired solar collectors energy efficiency improvement using inertial materials. In: Proceedings of the 8th International Conference on ENERGY and ENVIRONMENT (CIEM) 2017, 19–20 October 2017, Bucharest, Romania. https://doi:10.1109/CIEM.2017.8120775.

Bejan, A.S., Labihi, A., Croitoru, C.V., Catalina, T., Chehouani, H., Benhamou, B., 2018. Experimental investigation of the charge/discharge process for an organic PCM macroencapsulated in an aluminum rectangular cavity. In: EENVIRO 2017 Workshop - Advances in Heat and Transfer in Built Environment, E3S Web Conf. 32, 2018. https://doi.org/10.1051/e3sconf/20183201004.

Bejan, A.S., Tacutu, L., Croitoru, C.V., Nastase, I., 2018. Airflow study inside an enclosure with PCM wall and a solar collector. In: Proceedings of Roomvent & Ventilation 2018 – Excellent Indoor Climate and High Performing Ventilation, 2–5 June 2018, Espoo, Finland.

Bourdeau, L.E., 1980. Study of two passive solar systems containing phase change materials for thermal storage. In: Proceedings of the 5th National Passive Solar Conference (American Solar Energy Society), 19–26 October 1980, Amherst, Massachusetts, USA, pp. 298–301.

Chan, H.Y., Zhu, J., Ruslan, M.H., Sopian, K., Riffat, S., 2014. Thermal analysis of flat and transpired solar facades. Energy Procedia 48, 1345–1354. https://doi.org/10.1016/j.egypro.2014.02.152.

Ciriminna, R., Meneguzzo, F., Pecoraino, M., Pagliaro, M., 2017. Solar air heating and ventilation in buildings: A key component in the forthcoming renewable energy mix. Energy Technol. 5 (8), 1165–1172. https://doi.org/10.1002/ente.201600758.

Cordeau, S., Barrington, S., 2011. Performance of unglazed solar ventilation air preheaters for broiler barns. Sol. Energy 85 (7), 1418–1429. https://doi.org/10.1016/j.solener.2011.03.026.

Croitoru, C., Nastase, I., Voicu, I., Meslem, A., Sandu, M., 2016a. Thermal evaluation of an innovative type of unglazed solar collector for air preheating. Energy Procedia 85, 149–155. https://doi.org/10.1016/j.egypro.2015.12.285.

Croitoru, C.V., Nastase, I., Bode, F.I., Meslem, A., 2016b. Thermodynamic investigation on an innovative unglazed transpired solar collector. Sol. Energy 131, 21–29. https://doi.org/10.1016/j.solener.2016.02.029.

Dymond, C., Kutscher, C., 1997. Development of a flow distribution and design model for transpired solar collectors. Sol. Energy 60 (5), 291–300. https://doi.org/10.1016/S0038-092X(96)00157-0.

Entrop, A.G., Halman, J.I.M., Dewulf, G.P.M.R., Reinders, A.H.M.E., 2016. Assessing the implementation potential of PCMs: The situation for residential buildings in the Netherlands. Energy Procedia 96, 17–32. https://doi.org/10.1016/j.egypro.2016.09.090.

Exxon Mobil Corporation. 2019. 2019 - Outlook for Energy: A Perspective to 2040. Irving, Texas, USA. https://corporate.exxonmobil.com/Energy-and-environment/Looking-forward/Outlook-for-Energy/Outlook-for-Energy-A-perspective-to-2040.

Gielen, D., Boshell, F., Saygin, D., Bazilian, M.D., Wagner, N., Gorini, R., 2019. The role of renewable energy in the global energy transformation. Energy Strate. Rev. 24, 38–50. https://doi.org/10.1016/j.esr.2019.01.006.

Goyal, R.K., Tiwari, G.N., Garg, H.P., 1998. Effect of thermal storage on the performance of an air collector: A periodic analysis. Energy Convers. Manage. 39 (3–4), 193–202. https://doi.org/10.1016/S0196-8904(96)00226-9.

Gunnewiek, L.H., Hollands, K.G.T., Brundrett, E., 2002. Effect of wind on flow distribution in unglazed transpired-plate collectors. Sol. Energy 72 (4), 317–325. https://doi.org/10.1016/S0038-092X(02)00003-8.

Hami, K., Draoui, B., Hami, O., 2012. The thermal performances of a solar wall. Energy 39 (1), 11–16. https://doi.org/10.1016/j.energy.2011.10.017.

IEA – International Energy Agency, 2018. World Energy Outlook 2018. IEA, Paris, France https://www.iea.org/reports/world-energy-outlook-2018.

IEA – International Energy Agency, 2020. Global Energy Review 2020 - The impacts of the Covid-19 crisis on global energy demand and CO_2 emissions. IEA, Paris, France https://www.iea.org/reports/global-energy-review-2020.

Lai, C.M., Hokoi, S., 2015. Solar façades: A review. Build. Environ. 91, 152–165. https://doi.org/10.1016/j.buildenv.2015.01.007.

Leon, M.A., Kumar, S., 2007. Mathematical modeling and thermal performance analysis of unglazed transpired solar collectors. Sol. Energy 81 (1), 62–75. https://doi.org/10.1016/j.solener.2006.06.017.

Li, X., Zheng, S., Tian, G., Zhan, L., Yao, W., 2020. A new energy saving ventilation system assisted by transpired solar air collectors for primary and secondary school classrooms in winter. Build. Environ. 177, 106895. https://doi.org/10.1016/j.buildenv.2020.106895.

Moon, B.E., Kim, H.T., 2019. Evaluation of thermal performance through development of a PCM-based thermal storage control system integrated unglazed transpired collector in experimental pig barn. Sol. Energy 194, 856–870. https://doi.org/10.1016/j.solener.2019.11.009.

Navarro, L., de Gracia, A., Castell, A., Cabeza, L.F., 2016. Experimental study of an active slab with PCM coupled to a solar air collector for heating purposes. Energy Build. 128, 12–21. https://doi.org/10.1016/j.enbuild.2016.06.069.

Nkwetta, D.N., Haghighat, F., 2014. Thermal energy storage with phase change material—A state-of-the art review. Sustain. Cities Soc. 10, 87–100. https://doi.org/10.1016/j.scs.2013.05.007.

Paya-Marin, M.A., Lim, J.B.P., Chen, J.F., Lawson, R.M., Gupta, B.S., 2015. Large scale test of a novel back-pass non-perforated unglazed solar air collector. Renewable Energy 83, 871–880. https://doi.org/10.1016/j.renene.2015.05.039.

Paya-Marin, M.A., 2017. Solar Air Collectors for Cost-Effective Energy-Efficient Retrofitting. In: Pacheco-Torgal, F., Granqvist, C.G., Jelle, B.P., Vanoli, G.P., Bianco, N., Kurnitski, J. (Eds.), Cost-Effective Energy Efficient Building Retrofitting – Materials, Technologies, Optimization and Case Studies. Woodhead Publishing, Duxford (UK), pp. 141–168.

Peci, F., Taboas, F., Comino, F., Ruiz de Adana, M., 2020. Experimental study of a modular Unglazed transpired collector Façade for building refurbishment. Sol. Energy 201, 247–278. https://doi.org/10.1016/j.solener.2020.02.103.

Poole, M.R., Shah, S.B., Boyette, M.D., Stikeleather, L.F., Cleveland, T., 2018. Performance of a coupled transpired solar collector—phase change material-based thermal energy storage system. Energy Build. 161, 72–79. https://doi.org/10.1016/j.enbuild.2017.12.027.

Qiu, L., Ouyang, Y., Feng, Y., Zhang, X., 2019. Review on micro/nano phase change materials for solar thermal applications. Renewable Energy 140, 513–538. https://doi.org/10.1016/j.renene.2019.03.088.

Reichl, Ch., Kramer, K., Thoma, Ch., Benovsky, P., Lemée, T., 2015. Comparison of modelled heat transfer and fluid dynamics of a flat plate solar air heating collector towards experimental data. Sol. Energy 120, 450–463. https://doi.org/10.1016/j.solener.2015.07.011.

Rubitherm, 2019. RT35 Data Sheet. https://www.rubitherm.eu/media/products/datasheets/Techdata_-RT35_EN_06082018.PDF.

Shuklaa, A., Nkwetta, D.N., Cho, Y.J., Stevenson, V., Jones, P., 2012. A state of art review on the performance of transpired solar collector. Renew. Sustain. Energy Rev. 16 (6), 3975–3985. https://doi.org/10.1016/j.rser.2012.02.029.

Tajdaran, S., Kendrick, C., Hopkins, E., Bonatesta, F., 2020. Geometrical optimisation of Transpired Solar Collectors using design of experiments and computational fluid dynamics. Sol. Energy 197, 527–537. https://doi.org/10.1016/j.solener.2020.01.018.

Tyagi, V.V., Buddhi, D., 2007. PCM thermal storage in buildings: A state of art. Renew. Sustain. Energy Rev. 11 (6), 1146–1166. https://doi.org/10.1016/j.rser.2005.10.002.

UN Environment and International Energy Agency – IEA. 2017. Towards a zero-emission, efficient, and resilient buildings and construction sector. Global Status Report 2017. https://www.worldgbc.org/sites/default/files/UNEP%20188_GABC_en%20%28web%29.pdf.

US Energy Information Administration – EIA (US Department of Energy), 2019. International Energy Outlook 2019 with projections to 2050. Washington DC, USA. https://www.eia.gov/outlooks/ieo/pdf/ieo2019.pdf.

Wang, X., Bo, L., Bi, H., Yu, T., 2017. A simplified method for evaluating thermal performance of unglazed transpired solar collectors under steady state. Appl. Therm. Eng. 117, 185–192. https://doi.org/10.1016/j.applthermaleng.2017.01.053.

Weiss, W., Spörk-Dür, M., 2020. Solar Heat Worldwide, Global Market Development and Trends in 2019. Detailed Market Data 2018, AEE - Institute for Sustainable Technologies, Gleisdorf, Austria. https://www.iea-shc.org/Data/Sites/1/publications/Solar-Heat-Worldwide-2019.pdf.

Zhang, T.T., Tan, Y.F., Yang, H.X., Zhang, X.D., 2016a. The application of air layers in building envelopes: A review. Appl. Energy 165, 707–734. https://doi.org/10.1016/j.apenergy.2015.12.108.

Zhang, T.T., Tan, Y.F., Zhang, X.D., Li, Z.G., 2016b. A glazed transpired solar wall system for improving indoor environment of rural buildings in northeast China. Build. Environ. 98, 158–179. https://doi.org/10.1016/j.buildenv.2016.01.011.